Modified emission of extended light emitting layers by selective coupling to collective lattice resonances

Mohammad Ramezani,[1,*] Gabriel Lozano,[2,3] Marc A. Verschuuren,[4] and Jaime Gómez-Rivas[1,5]

[1]*FOM Institute DIFFER, P.O. Box 6336, 5600 HH Eindhoven, The Netherlands*

[2]*Center for Nanophotonics, FOM Institute AMOLF, c/o Philips Research Laboratories, High Tech Campus 4, 5656 AE Eindhoven, The Netherlands*

[3]*Institute of Materials Science of Seville, Spanish National Research Council-University of Seville, Avenida Americo Vespucio 49, 41092 Seville, Spain*

[4]*Philips Group Innovation, Intellectual Property & Standards, High Tech Campus 4, 5656 AE, Eindhoven, The Netherlands*

[5]*COBRA Research Institute, Eindhoven University of Technology, P.O. Box 513, 5600 MB Eindhoven, The Netherlands*

(Received 18 May 2016; revised manuscript received 13 August 2016; published 6 September 2016)

We demonstrate that the coupling between light emitters in extended polymer layers and modes supported by arrays of plasmonic particles can be selectively enhanced by accurate positioning of the emitters in regions where the electric field intensity of a given mode is maximized. The enhancement, which we measure to reach up to 70%, is due to the improved spatial overlap and coupling between the optical mode and emitters. This improvement of the coupling leads to a modification of the emission spectrum and the luminous efficacy of the sample.

DOI: 10.1103/PhysRevB.94.125406

I. INTRODUCTION

Resonant metallic nanoparticles have been the subject of many studies in recent years due to their ability to enhance and confine electromagnetic fields in subwavelength volumes. These characteristics originate from coherent oscillations of free charges confined in the nanoparticles, termed as localized surface plasmon resonances (LSPRs) [1]. In addition to LSPRs, periodic arrays of metallic nanoparticles can support collective lattice resonances [2,3]. These lattice resonances originate from the radiative coupling between LSPRs, enhanced by diffracted orders in the plane of the array or by refractive index guided modes in the proximity of the array. In the former case the collective resonances are known as surface lattice resonances (SLRs) [2,4–9], while the latter are known as waveguide-plasmon polaritons [10,11] or quasiguided modes [12], depending on the degree of coupling between the localized resonances and the waveguide modes. In contrast to LSPRs, collective resonances are characterized as being weakly confined to the nanoparticles, i.e., having a large extension into the surrounding media [7,13]. This feature of lattice resonances is a consequence of their hybrid photonic-plasmonic nature [12]. The delocalization of the electric field leads to a reduction of Ohmic losses in the metal, while destructive interference of the light scattered to the far field reduces the radiation damping, which results in resonances with higher quality factors [2,14]. The use of these phenomena has led to linewidths in hybrid photonic-plasmonic resonances as narrow as 1 nm and resonance Q factors of 400 [15]. Due to the improved characteristics of lattice resonances, they have been proposed for applications such as sensing [16,17], spectroscopy [18], surface-enhanced Raman spectroscopy [19,20], solid-state lighting [11,21–23], and lasing [24,25]. Indeed, light emitters in the proximity of nanoparticle arrays can couple to collective resonances, resulting in a modification of their emission. This coupling leads to spectral reshaping [7,26], changes in the directionality [27] and polarization of the emission [28], and a modified spontaneous decay rate accounting for the change of the optical density of states [29–31]. There are several parameters that influence the coupling of the light emitters to the optical resonances, including their dipole moment orientation, the transition frequency, and the spatial overlap between the light emitters and the local electric field associated with the resonance.

In this paper, we demonstrate the control of the emission from extended luminescent layers by controlling the spatial overlap between the resonant field associated with collective lattice resonance and the light emitters. This control is achieved by the selective placement of the emitters at a defined distance from the nanoparticle array, and the subsequent variation of their position relative to the array. The selective localization of the emitters enables a preferential coupling of the emission to a certain collective resonance by maximizing the spatial overlap of the emitters with the electric field of the collective resonances. This approach results in an improved emission in the forward direction with engineered spectrum. It also defines a path in the design of plasmonic-based color-converting layers that can be used in white-light-emitting devices with improved directional emission and brightness [22].

II. FABRICATION OF NANOPARTICLE ARRAY AND CHARACTERIZATION

Periodic arrays of aluminum nanoparticles with a size of $3 \times 3\ \mathrm{mm}^2$ have been fabricated onto a fused silica substrate by substrate conformal nanoimprint lithography (SCIL) followed by reactive ion etching (RIE) of the aluminum. SCIL enables the fabrication of large-area samples with high reproducibility [32,33]. Figure 1(a) shows a top view SEM image of the aluminum array. The structure consists of a hexagonal array of nanoparticles with a lattice constant of 475 nm. The nanoparticles have the shape of pyramids with a height of

*m.ramezani@differ.nl

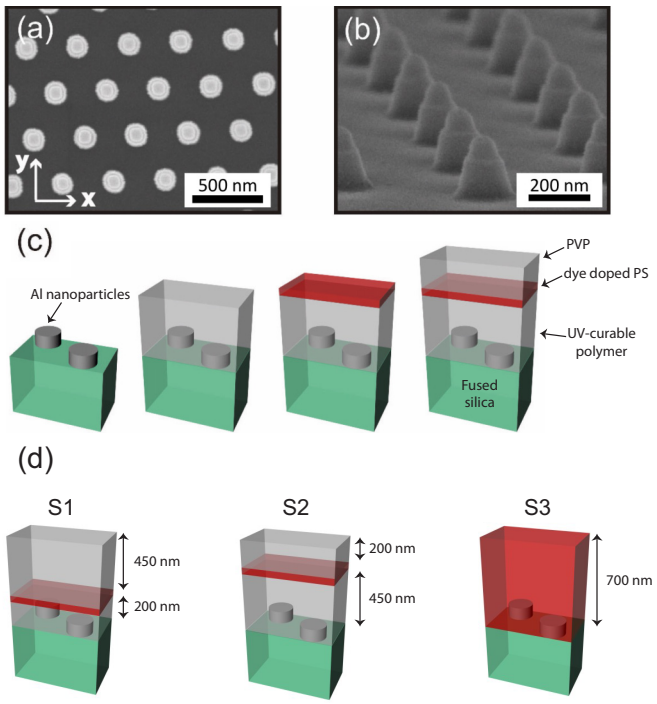

FIG. 1. (a) Top view SEM image of a hexagonal array of aluminum nanoparticles with a lattice constant of 475 nm. (b) Side view of the same array. (c) Sketch of the fabrication process of a multilayered luminescent layer on the metallic structure. Fused silica substrate is shown in green. The Al nanoparticles are represented in dark gray. Transparent UV-curable polymer and PVP polymer are shown in light gray within the luminescent layer. The thin film of polystyrene (PS) containing the dye molecules is indicated as a red layer. (d) The structure of the three investigated samples with positioned emitters in different regions.

150 nm and diameter of 80 nm at the top and of 140 nm at the bottom. Each particle is coated by a thin layer of native oxide (Al_2O_3) that protects the particles from further oxidation. In Fig. 1(b) a side view of the array is shown. The step around the apex of each particle is due to the two-step etching process applied during the fabrication procedure in order to etch the sol-gel mask on top of the aluminum layer [32,34].

In order to position the emitters at defined heights relative to the nanoparticles, three different polymer layers with a total height of 700 nm were spin coated on the arrays. The fabrication steps are illustrated schematically in Fig. 1(c). The schematic representation of the three investigated samples with positioned emitters is displayed in Fig. 1(d). In the first sample, named S1, the lowest layer has a thickness of 200 nm and consists of a transparent UV-curable polymer (Norland 61) with a refractive index of 1.52, which was dissolved in toluene for spin coating. A second layer with a thickness of 50 nm of polystyrene (refractive index 1.59) containing 3 wt. % organic emitters (highly efficient Lumogen F305, BASF) is spin coated on top. For the uppermost layer, polyvinylpyrrolidone (PVP) of refractive index 1.56 was spin coated on top of the polystyrene layer with a thickness of 250 nm [see Fig. 1(d), left]. Another sample, named S2, was prepared using the same method; however, the thickness of the layers was varied to locate the dye molecules at the height between 450 nm and 500 nm.

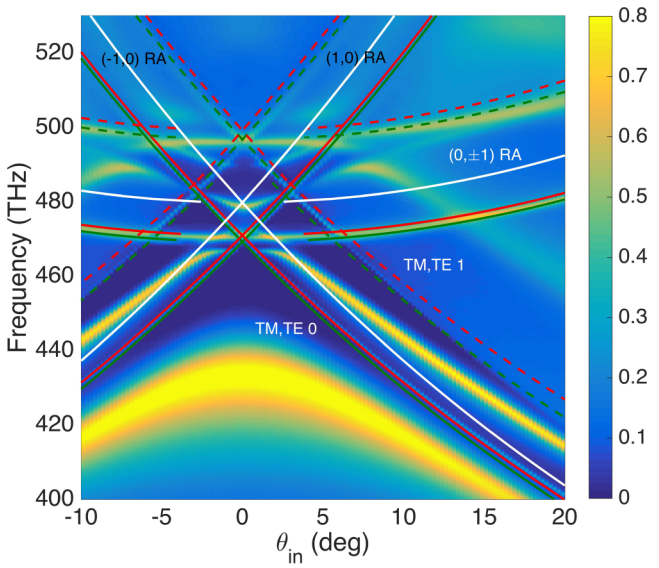

FIG. 2. Angle-resolved extinction map measured with *s*-polarized incident light. The solid white lines correspond to the dispersion of Rayleigh anomalies in a homogeneous medium with refractive index of 1.52. The solid green (TE) and red (TM) lines indicate the position of zeroth-order quasiguided modes. The dashed lines are higher order quasiguided modes.

In this sample, the Norland 61 polymer with a thickness of 450 nm was spin coated, on top of which was the 50 nm layer of the polystyrene containing the dye molecules. The upper 200 nm thick layer was made of PVP to achieve a total layer thickness of 700 nm [see Fig. 1(d), middle]. In order to compare the emission of the samples with positioned emitters with a sample containing emitters homogeneously distributed over the full layer, a third sample, named S3, was fabricated with a polystyrene layer with a thickness of 700 nm over the particle array containing 3 wt. % dye molecules [see Fig. 1(d), right]. In the first two samples the thin layers are formed by three different polymers. The reason for selecting different polymers is to avoid dissolving or damaging the underlying layer due to the contact with the solvent of the next layer.

We have performed extinction measurements to resolve the different resonances in the samples, using a collimated linearly polarized white-light beam generated with a halogen lamp (Energetiq Technology). The incident beam is *s*-polarized (polarization along the y axis) and the sample is rotated along the y axis [see Fig. 1(a)]. The transmittance in the direction of the incident beam (zero-order transmittance, T_0) is collected by a lens ($f = 5$ cm) focusing the light into a multimode optical fiber with a 400 μm core diameter and measured with a spectrometer (Ocean Optics USB2000+) at each angle of incidence. The extinction is defined as $1 - T_0$. Figure 2 displays the extinction spectra of S3 as a function of the angle of incidence. To correlate the features in the extinction spectra shown in Fig. 2 with collective lattice resonances supported by the array, we calculate the Rayleigh anomalies (RAs), i.e., the dispersion of diffracted orders grazing to the plane of the array, using the grating equation

$$\pm\vec{k}_{\|d} = \vec{k}_{\|i} \pm \vec{G}, \tag{1}$$

where $\vec{k}_{\|d} = \frac{2\pi}{\lambda} n_{\text{eff}} \hat{u}_d$ and $\vec{k}_{\|i} = \frac{2\pi}{\lambda} \sin(\theta) \hat{u}_i$ are the parallel components of the diffracted and incident wave vectors, respectively ($\hat{u}_d$ and $\hat{u}_i$ are the unitary vectors along the diffracted and incident directions), $\vec{G}$ is the reciprocal lattice vector of the hexagonal array, θ is the angle between the wave vector of the incident beam and the direction normal to the sample, and n_{eff} is the effective index defining the phase velocity of the in-plane diffracted wave, i.e., the RAs. RAs are responsible for the enhanced radiative coupling of LSPRs, which leads to SLRs [5]. Therefore, the dispersion of SLRs should be similar to that of the RAs. In this structure, assigning the value of n_{eff} for the in-plane diffracted wave is not straightforward, since the surrounding medium of the particles is inhomogeneous due to the presence of the substrate. For the calculation, we assume an average effective refractive index n_{eff} of 1.52. The dispersions of (± 1, 0) and (0, ± 1) RAs are shown in Fig. 2 with solid white lines.

Along with the RAs, we calculate the dispersion of the quasiguided modes in the polymer supported by this multilayered medium. The details of the quasiguided-mode calculations can be found in Refs. [23,35,36]. The red (TM) and green (TE) solid lines correspond to the zeroth-order quasiguided modes coupled into free space through the (1, 0), (-1, 0), and (0, ± 1) diffracted orders. Also, the first-order quasiguided modes are shown in the same figure by the red and green dashed lines. As can be seen in Fig. 2, a good agreement between the calculated dispersions and the extinction measurement is obtained. However, we should consider that these calculations are based on the empty-lattice approximation in which the coupling between modes is neglected [37]. This coupling can partially explain the discrepancies between measurements and calculations.

To study the effect of the spatial overlap between the different collective modes of the array and the emitters on the directionality of the emission and photoluminescence enhancement in the forward direction, we focus on the direction normal to the array. Figures 3(a)–3(c) display the extinction measurements at normal incidence of the array with the dye layer at a height of 225 ± 25 nm (S1), the array with the dye layer at a height of 475 ± 25 nm (S2), and the array fully covered with dye molecules (S3), respectively. In all the measurements, three narrow resonances and one broad peak are clearly distinguishable. The narrow resonances can be assigned to the collective resonances supported by the arrays and the broad peak can be attributed to the localized surface plasmon resonance in the individual nanoparticles. In the extinction measurements of the samples with emitters localized at the defined heights, i.e., S1 and S2 [Figs. 3(a) and 3(b)], there are small shifts in the frequency of the peaks relative to S3. These shifts can be explained by the small change of the effective refractive index in the multilayered samples due to the different polymers that have been used.

To gain more physical insight into the extinction measurements, we have performed finite-difference time domain (FDTD) simulations of the extinction. The optical constants of the aluminum and fused silica used in the simulations are obtained from the literature [38]. The simulations of the extinction of the three samples are displayed in Figs. 3(a)–3(c)

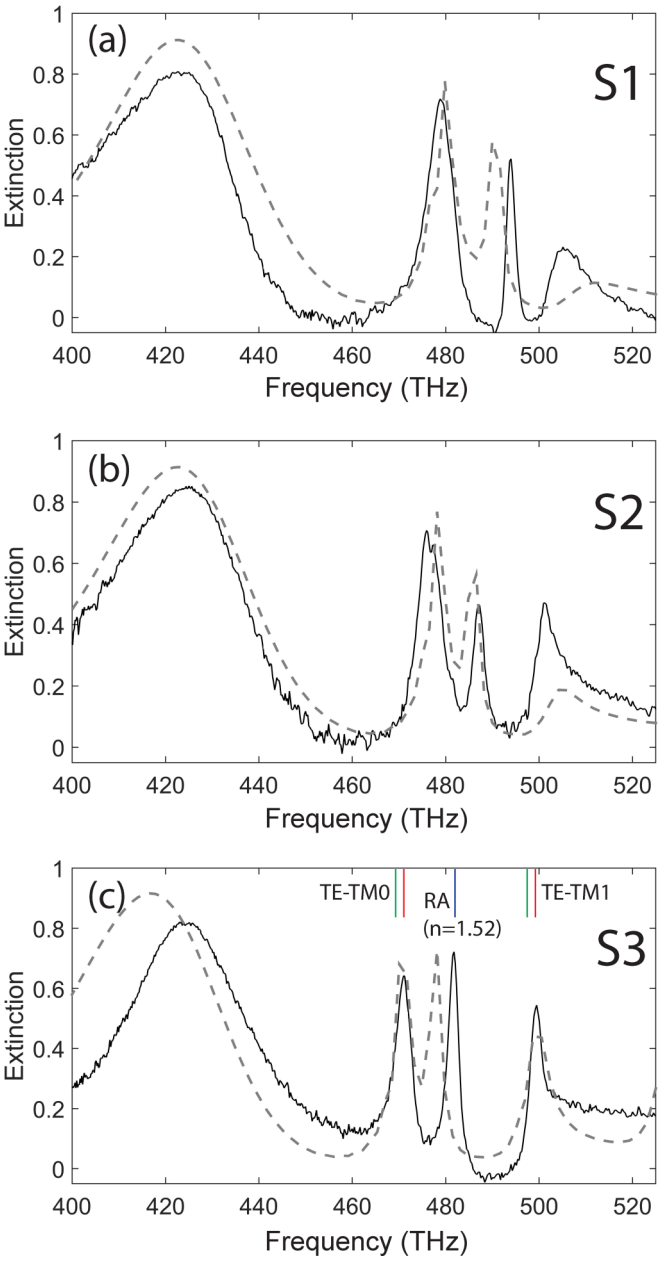

FIG. 3. Measured (solid) and simulated (dashed) extinction spectra at normal incidence with the luminescent layer covering the array with the thickness of 700 nm. (a) The sample with 50 nm layer doped with the dye at 225 ± 25 nm (S1). (b) The sample with 50 nm layer doped with the dye at 475 ± 25 nm (S2). (c) The sample with the dye randomly distributed all over the polymer layer (S3).

as dashed lines, where we see a good agreement with the experiments. At this point, we stress that the extinction spectra for the three samples are very similar. These similar spectra are expected because of the low concentration of dye molecules, which do not introduce significant changes in the permittivity of the layers. In order to have a better insight on the modes supported by the array and their electric field distributions, the simulated electric field intensity enhancement in the layer at each resonant frequency is depicted in Fig. 4. In this figure, the local field intensity enhancement (relative to the incident

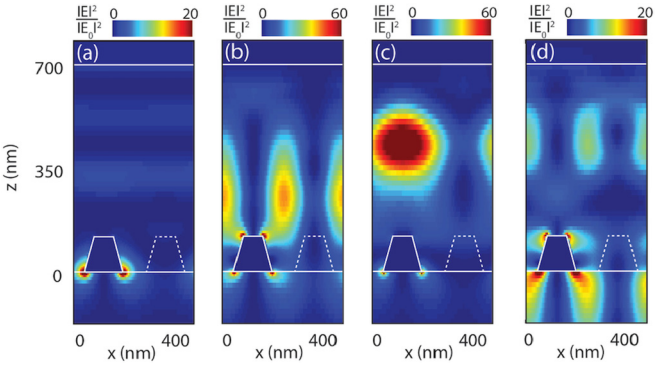

FIG. 4. Three-dimensional FDTD simulations of the spatial distribution of the electric field $|E|^2$ normalized by the incident field intensity $|E_0|^2$ for a hexagonal array fabricated on a silica substrate with refractive index of 1.46, and covered by 700 nm layer of polymer with a refractive index of 1.59. This structure corresponds to S3. Similar field distributions are expected for S1 and S2 due to the similar refractive indexes of the different layers. Simulations are performed considering that the array is illuminated with a plane wave at normal incidence with a wavelength of (a) $\nu_1 = 416$ THz, (b) $\nu_2 = 469$ THz, (c) $\nu_3 = 483$ THz, and (d) $\nu_4 = 499$ THz. Results are shown in the xz plane of a unit cell of the array. The nanoparticles and the different dielectric interfaces are marked using white lines.

intensity) for a plane wave at normal incidence is shown. The nanoparticle boundaries and the interfaces between the different dielectric layers are represented by white lines in Fig. 4, while the dashed lines indicate the boundary of the nanoparticle in the back plane. Strong variations in the spatial distribution of electric field intensity can be seen for the different frequencies. The three narrow peaks at $\nu = 469$ THz (ν_2), $\nu = 483$ THz (ν_3), and $\nu = 499$ THz (ν_4) in the extinction are associated with the collective resonances arising from the periodic array and the layered waveguide system. As mentioned earlier, at the frequency of the collective resonances, the electric field intensity is enhanced and extends out of the plane of the particle array. The distinctive characteristic of the collective resonances is the enhancement of the electric fields in large volumes compared to the LSPRs in the vicinity of individual particles. This can be clearly appreciated by comparing their field profiles with that of the LSPRs on the metallic particles, i.e., the field profile at $\nu = 416$ THz (ν_1) [Fig. 4(a)], which shows the highly localized and strong field enhancement at the bottom of the particle.

III. PHOTOLUMINESCENCE ENHANCEMENT OF THE SAMPLES WITH POSITIONED EMITTERS

As previously discussed, in order to maximize the coupling of the emission to the collective resonances of the array, it is necessary to maximize the spatial and spectral overlap between the emitters and the resonances. We can satisfy the spectral overlap by choosing emitters that are luminescent in the frequency range of the resonance. However, due to the heterogeneous spatial distribution of the electric field, most of the emitters that are homogeneously distributed over the polymer layer will not efficiently couple to the resonances.

The photoluminescence (PL) spectrum in the normal direction was measured for each sample to investigate the effect of localizing the emitters at different positions across the layer and the impact of this localization on the improvement of the emission. A continuous-wave diode laser emitting at the wavelength of 453 nm (661 THz) is used to excite the sample at an incidence angle of 10 degrees. In Figs. 5(a) and 5(b), the PL spectra of the samples with the emitters at $h = 225 \pm 25$ nm (S1) and at $h = 475 \pm 25$ nm (S2) are shown, respectively. The emission of a bare layer of the emitters with the same thickness but without the nanoparticle array is displayed as the brown shaded area in each panel. A strong spectral reshaping of the emission, which is different for the two samples, can be observed.

To illustrate the effect of localizing the emitters at the defined height and their spatial overlap with the different modes of the sample, we have determined the photoluminescence enhancement (PLE). The PLE is defined as the ratio between the emission of the emitters on top of the nanoparticle array to the emission of a similar layer without the presence of nanoparticles (reference layer). The spectrally resolved PLE measurements of three samples are shown in Figs. 6(a)–6(c). By changing the height of the thin layer of the dye molecules across the polymer layer, the PLE spectrum changes significantly as a consequence of the coupling of the emission to different modes. As mentioned earlier in the description of extinction measurements, due to the use of different polymers with slightly different refractive indices, small shifts in the frequency of each peak with respect to the frequency of the similar peak in the other samples is observed.

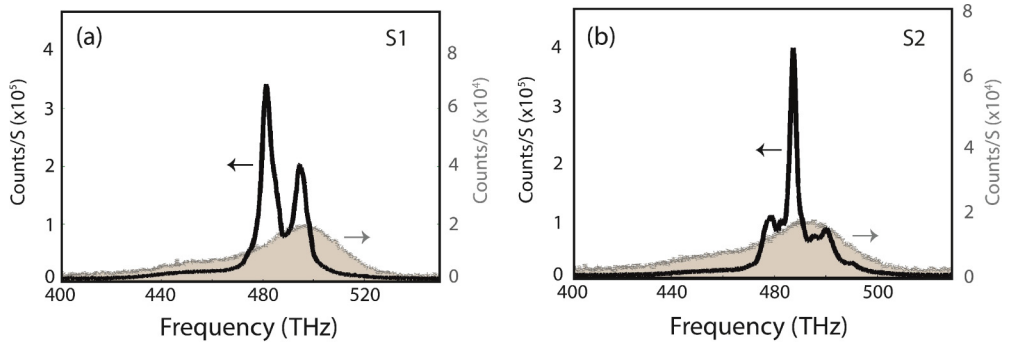

FIG. 5. PL spectra for the samples with the dye layer between (a) 225 ± 25 nm (S1) and (b) 475 ± 25 nm (S2). The PL of the dye layer in the absence of the plasmonic array is shown as the brown shaded area in each case.

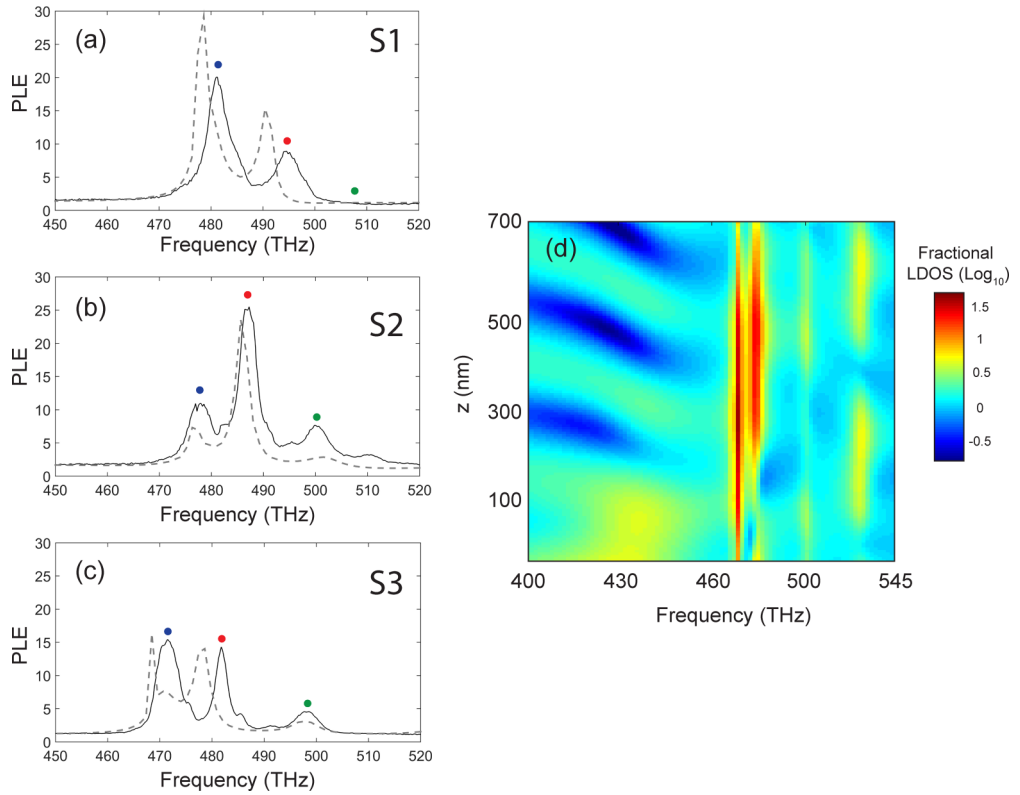

FIG. 6. Measurements of the photoluminescence enhancement (solid) and simulations of the intensity enhancement, i.e., integrated total electric field intensity (dashed) for a hexagonal array covered by a polymer layer as a function of the free-space frequency for the sample with 50 nm layer of the polystyrene containing the dye at height (a) 225 ± 25 nm (S1) and (b) 475 ± 25 nm above the substrate (S2) and (c) the sample with 700 nm layer of polystyrene containing the dye (S3). The schematic representations of the structure for different samples are shown in the inset of each panel. (d) The map of the calculated fractional RLDOS normalized by the fractional RLDOS of the polymer layer without the nanoparticle for the forward direction.

In Figs. 6(a)–6(c) we have marked the same modes by dots with similar colors for different samples. Two strong peaks of enhanced PL at $\nu = 471$ THz and $\nu = 481$ THz and one less pronounced peak at $\nu = 497$ THz are visible in the emission of S3. The PL is enhanced by a factor of 15 at $\nu = 471$ THz and 14 at $\nu = 481$ THz with respect to the reference. By positioning the emitters at a height of 225 ± 25 nm (S1), the PLE at $\nu = 481$ THz is lowered to a value of 9. In exchange, the PLE at $\nu = 471$ THz is intensified up to 21 times. Similarly, by positioning the emitters at a height of 475 ± 25 nm (S2), it is possible to increase the PLE at $\nu = 481$ nm from 14 to 24 that corresponds to 70% increase with respect to S1. At the same time, the PLE at $\nu = 471$ THz drops from a value of 15 to 10.

In order to describe the changes in PLE, we make use of the Lorentz reciprocity theorem and calculate the electric field intensity in the layer when it is illuminated by a plane wave in the same direction at which the photoluminescence was measured. By reciprocity, the local intensity enhancement of the field component along the orientation of the dipole moment at the position of the emitter is proportional to the dipole emission probability in the direction of illumination. The local intensity enhancement can be defined as the fractional radiative local density of states (RLDOS) in that direction. The total intensity enhancement (IE) is defined as the integral of the intensity enhancement over the volume occupied by the emitters:

$$\mathrm{IE}(\nu,\Omega) = \frac{\int_V |E(x,y,z,\nu,\Omega)|^2 dV}{\int_V |E_{ref}(x,y,z,\nu,\Omega)|^2 dV}, \qquad (2)$$

where Ω is the solid angle given by the elevation and the azimuthal angle of emission, $E(x,y,z,\nu,\Omega)$ is the local electric field at the wavelength ν and at the spatial position (x,y,z) where each emitter is located, and $E_{ref}(x,y,z,\nu,\Omega)$ is the local field intensity in the absence of the nanoparticle array. For each sample, the volume is defined as a region within the polymer where the emitters are positioned. Simulations of the IE for the three different samples in our study are shown in Figs. 6(a)–6(c) as dashed lines. An excellent agreement between the simulations and the experimental results is obtained, confirming that the inhomogeneous field distribution across the polymer layer on top of the nanoparticle array is responsible for the differences in the emission.

We have calculated the IE for all the intermediate heights and as a function of the emission frequency. These calculations are displayed in Fig. 6(g). Through this figure we can quantitatively assign the out-coupling efficiency of the emission in the forward direction from sources located at different heights and emitting at different frequencies. For instance, to efficiently couple the emission to the mode radiating at $\nu = 469$ THz, the emitters should be placed between the heights of $z = 50$ nm and 600 nm. Similarly, for the resonance at $\nu = 481$ THz

the optimum height with the highest coupling efficiency is between $z = 200$ nm and 600 nm. In the frequency range from $\nu = 450$ THz to $\nu = 460$ THz, an oscillation in the IE is observed, which corresponds to the Fabry-Pérot resonance in the polymer layer. At $\nu = 430$ THz, a moderate enhancement of the IE is visible at small heights. This enhancement corresponds to the LSPRs in the individual nanoparticles.

IV. SPECTRAL LUMINOUS EFFICACY

The ability to control the emission spectrum of sources by their coupling to defined modes represents an interesting approach to improve the efficacy of light sources. The emission of the investigated dye extends beyond $\nu = 428$ THz; however, the array has been designed such that it mainly modifies the emission in the spectral range 460 THz $< \nu <$ 500 THz, i.e., the red range of the visible spectrum where the human eye is most sensitive. In order to quantify the impact of the change in the spectral content of the emission, we determine the red luminous efficacy (η) in the direction defined by the solid angle Ω as the ratio between the luminous flux and the spectral power density. One must note that, unlike for the spectral luminous efficacy where the integration is performed over the entire visible range, the red luminous efficacy is integrated over a narrower range of frequencies within the red part of the spectrum [39]. The luminous efficacy defines how well a source produces visible light as perceived by the human eye, and can be expressed as

$$\eta(\Omega) = 683 \frac{\int J(\nu,\Omega)\bar{y}(\nu)d\nu}{\int J(\nu,\Omega)d\nu}, \tag{3}$$

where $J(\nu,\Omega)$ is the spectral power density, which is proportional to the emitted intensity in the solid angle Ω per unit time at frequency ν. The factor of 683 in Eq. (3), with units of lumens per watt, scales the luminous efficacy with the definition of lumen, and $\bar{y}(\nu)$ is the photopic sensitivity curve of the eye. The integrals are defined in the range of frequencies at which the source emits.

The calculated η for the dye layer at the height of 225 ± 25 nm in the emission range of the dye, i.e., between 352 THz and 599 THz, and in the normal direction, is 265 lm/W. This value becomes 269 lm/W when the emission is modified by the metal nanoparticle array (S1), which represents a negligible variation of the luminous efficacy. By positioning the layer of dye at the height of 475 ± 25 nm, η for the bare layer becomes 266 lm/W. This value is very close to the luminous efficacy measured for bare layer of the dye in the previous sample due to the unchanged emission profile. η increases to 294 lm/W by introducing the plasmonic array (S2), which represents a 10% enhancement with respect to the bare layer.

V. CONCLUSION

In conclusion, we have demonstrated that by positioning emitters at different heights with respect to an array of metallic nanoparticles it is possible to strongly modify their emission spectrum. This modification is caused by the different coupling of the emission to collective resonances supported by the array. These resonances are characterized by delocalized field distributions, which significantly enhance the emission in the forward direction. The precise positioning of the emitters favors the coupling of the emission to certain modes that are preferentially coupled out into free space by the array.

ACKNOWLEDGMENTS

This research was financially supported by the Nederlandse Organisatie voor Wetenschappelijk Onderzoek (NWO) through the project LEDMAP of the Technology Foundation STW and through the Industrial Partnership Program Nanophotonics for Solid State Lighting between Philips and the Foundation for Fundamental Research on Matter FOM. This work is also supported by NanoNextNL, a micro- and nanotechnology consortium of the Government of the Netherlands and 130 partners.

[1] P. Bharadwaj, R. Beams, and L. Novotny, Chem. Sci. **2**, 136 (2011).
[2] S. Zou and G. C. Schatz, J. Chem. Phys. **121**, 12606 (2004).
[3] F. J. García de Abajo, Rev. Mod. Phys. **79**, 1267 (2007).
[4] V. G. Kravets, F. Schedin, and A. N. Grigorenko, Phys. Rev. Lett. **101**, 087403 (2008).
[5] B. Auguié and W. L. Barnes, Phys. Rev. Lett. **101**, 143902 (2008).
[6] Y. Chu, E. Schonbrun, T. Yang, and K. B. Crozier, Appl. Phys. Lett. **93**, 181108 (2008).
[7] G. Vecchi, V. Giannini, and J. Gómez Rivas, Phys. Rev. Lett. **102**, 146807 (2009).
[8] B. Auguié, X. M. Bendaña, W. L. Barnes, and F. J. García de Abajo, Phys. Rev. B **82**, 155447 (2010).
[9] A. D. Humphrey and W. L. Barnes, Phys. Rev. B **90**, 075404 (2014).
[10] A. Christ, S. G. Tikhodeev, N. A. Gippius, J. Kuhl, and H. Giessen, Phys. Rev. Lett. **91**, 183901 (2003).
[11] S. R. K. Rodriguez, S. Murai, M. A. Verschuuren, and J. G. Rivas, Phys. Rev. Lett. **109**, 166803 (2012).
[12] S. Murai, M. A. Verschuuren, G. Lozano, G. Pirruccio, S. R. K. Rodriguez, and J. Gómez Rivas, Opt. Express **21**, 4250 (2013).
[13] G. Pirruccio, M. Ramezani, Said Rahimzadeh-Kalaleh Rodriguez, and J. G. Rivas, Phys. Rev. Lett. **116**, 103002 (2016).
[14] T. V. Teperik and A. Degiron, Phys. Rev. B **86**, 245425 (2012).
[15] A. Abass, S. R. K. Rodriguez, J. Gómez Rivas, and B. Maes, ACS Photonics **1**, 61 (2014).
[16] P. Offermans, M. C. Schaafsma, S. R. K. Rodriguez, Y. Zhang, M. Crego-Calama, S. H. Brongersma, and J. Gómez Rivas, ACS Nano **5**, 5151 (2011).
[17] A. I. Kuznetsov, A. B. Evlyukhin, M. R. Gonçalves, C. Reinhardt, A. Koroleva, M. L. Arnedillo, R. Kiyan, O. Marti, and B. N. Chichkov, ACS Nano **5**, 4843 (2011).
[18] R. Adato, A. A. Yanik, J. J. Amsden, D. L. Kaplan, F. G. Omenetto, M. K. Hong, S. Erramilli, and H. Altug, Proc. Natl. Acad. Sci. USA **106**, 19227 (2009).

[19] K. T. Carron, H. W. Lehmann, W. Fluhr, M. Meier, and A. Wokaun, J. Opt. Soc. Am. B **3**, 430 (1986).
[20] S. Zou and G. C. Schatz, Chem. Phys. Lett. **403**, 62 (2005).
[21] K. H. Cho, J. Y. Kim, D.-G. Choi, K.-J. Lee, J.-H. Choi, and K. C. Choi, Opt. Lett. **37**, 761 (2012).
[22] G. Lozano, D. J. Louwers, S. R. K. Rodriguez, S. Murai, O. T. A. Jansen, M. A. Verschuuren, and J. Gómez Rivas, Light: Sci. Appl. **2**, e66 (2013).
[23] K. Guo, G. Lozano, M. A. Verschuuren, and J. Gómez Rivas, J. Appl. Phys. **118**, 073103 (2015).
[24] W. Zhou, M. Dridi, J. Y. Suh, C. H. Kim, D. T. Co, M. R. Wasielewski, G. C. Schatz, and T. W. Odom, Nat. Nanotechnol. **8**, 506 (2013).
[25] A. H. Schokker and A. F. Koenderink, Phys. Rev. B **90**, 155452 (2014).
[26] V. Giannini, G. Vecchi, and J. Gómez Rivas, Phys. Rev. Lett. **105**, 266801 (2010).
[27] S. R. K. Rodriguez, G. Lozano, M. A. Verschuuren, R. Gomes, K. Lambert, B. De Geyter, A. Hassinen, D. Van Thourhout, Z. Hens, and J. Gómez Rivas, Appl. Phys. Lett. **100**, 111103 (2012).
[28] M. Cotrufo, C. I. Osorio, and A. F. Koenderink, ACS Nano **10**, 3389 (2016).
[29] G. Pellegrini, G. Mattei, and P. Mazzoldi, J. Phys. Chem. C **115**, 24662 (2011).
[30] R. Guo, S. Derom, A. I. Väkeväinen, R. J. A. van Dijk-Moes, P. Liljeroth, D. Vanmaekelbergh, and P. Törmä, Opt. Express **23**, 28206 (2015).
[31] K. Guo, M. A. Verschuuren, and A. F. Koenderink, Optica **3**, 289 (2016).
[32] M. A. Verschuuren, Substrate conformal imprint lithography for nanophotonics, Ph.D. thesis, Utrecht University, 2010.
[33] R. Ji, M. Hornung, M. A. Verschuuren, R. van de Laar, J. van Eekelen, U. Plachetka, M. Moeller, and C. Moormann, Microelectron. Eng. **87**, 963 (2010).
[34] G. Lozano, G. Grzela, M. A. Verschuuren, M. Ramezani, and J. Gómez-Rivas, Nanoscale **6**, 9223 (2014).
[35] M. Born and E. Wolf, *Principles of Optics* (Cambridge University Press, 1999).
[36] P. Yeh, *Optical Waves in Layered Media* (Wiley, 2005).
[37] S. G. Tikhodeev, A. L. Yablonskii, E. A. Muljarov, N. A. Gippius, and T. Ishihara, Phys. Rev. B **66**, 045102 (2002).
[38] E. D. Palik, *Handbook of Optical Constants of Solids* (Academic Press, 1985).
[39] A. Nikitin, M. Ramezani, and J. Gómez Rivas, ECS J. Solid State Sci. Technol. **5**, R3164 (2016).